

Design study of random spectrometers for applications at optical frequencies

PARIS VARYTIS^{1*}, DAN-NHA HUYNH², WLADISLAW HARTMANN^{3,4}, WOLFRAM PERNICE^{3,4}, AND KURT BUSCH^{1,2}

¹Max-Born-Institut, Max-Born-Str. 2A, 12489 Berlin, Germany

²Humboldt-Universität zu Berlin, Institut für Physik, AG Theoretische Optik & Photonik, Newtonstr 15, 12489 Berlin, Germany

³University of Münster, Institute of Physics, Wilhelm-Klemm-Str. 10, 48149 Münster, Germany

⁴University of Münster, CeNTech - Center for Nanotechnology, Heisenbergstr. 11, 48149 Münster, Germany

* Corresponding author: varytis@physik.hu-berlin.de

Compiled February 15, 2022

Compact spectrometers based on disordered planar waveguides exhibit a rather high resolution with a relatively small footprint as compared to conventional spectrometers. This is achieved by multiple scattering of light which – if properly engineered – significantly enhances the effective optical path length. Here a design study of random spectrometers for TE- and TM-polarized light is presented that combines the results of Mie theory, multiple-scattering theory and full electromagnetic simulations. It is shown that the performance of such random spectrometers depends on single scattering quantities, notably on the overall scattering efficiency and the asymmetry parameter. Further, the study shows that a well-developed diffusive regime is not required in practice and that a standard integrated-optical layout is sufficient to obtain efficient devices even for rather weakly scattering systems consisting of low index inclusions in high-index matrices such as pores in planar silicon-nitride based waveguides. This allows for both significant reductions in footprint with acceptable losses in resolution and for device operation in the visible and near-infrared frequency range.

OCIS codes: (290.1990) Diffusion; (290.4020) Mie theory; (290.4210) Multiple scattering; (300.6190) Spectrometers

<http://dx.doi.org/10.1364/ao.XX.XXXXXX>

Random spectrometers are suitable for portable sensing and efficient lab-on-a-chip functionality. While previous efforts aimed at the telecom wavelength regime with silicon-based structures [1], random spectrometers operating in the near-infrared (NIR) spectral region where water, cells and tissue exhibit low absorption (and molecules feature low fluorescence) could offer important advantages for biological and medical applications such as Raman spectroscopy [2] and bioimaging [3, 4]. Similar arguments can be made with respect to operations at visible frequencies.

In the present work, we analyze the performance of planar

random spectrometers for frequencies in the visible, NIR and telecom ranges for both polarizations (TE and TM) by means of Mie and multiple-scattering theory in conjunction with the numerical solution of the Maxwell equations. To provide the required broadband optical transparency, we conduct our design study for silicon-nitride based waveguides. In fact, silicon nitride is a robust material [5, 6] with low thermal sensitivity that is compatible with CMOS processes for low-cost mass fabrication. Further, silicon nitride is transparent in the wavelength regime between 700 nm and 1100 nm where it features a relatively high refractive index ($n \sim 2$) so that it is suitable for many applications in the visible and NIR regime [7–10]. As scattering area, we consider a set of identical pores that have been etched into the silicon nitride waveguide.

In Fig. 1 we depict the considered random spectrometer geometry: We use a semicircular scattering area with a radius of $L = 25 \mu\text{m}$, which consists of a random array of identical pores with 125 nm radius that cover 9 % of the scattering area. A single input waveguide (with a width of $2 \mu\text{m}$) launches light into the center of the scattering area and after multiple scattering light reaches the 13 readout waveguides (with widths of $2 \mu\text{m}$), which are placed with equal angular distance around the outer circumference. The backscattering into the launch waveguide provides the 14th readout port. Into this two-dimensional system, we launch a fundamental mode pulse, and at the locations of the detectors D_1, \dots, D_{13} we determine the radiation that exits through the readout port. After a Fourier transform of the (time-dependent) output signals, we recover the frequency-resolved transmission matrix T with a single time-domain computation. For the actual numerical computations we utilize a Discontinuous Galerkin Time-Domain (DGTD) finite-element approach [11, 12].

To quantify the spectral resolution of the spectrometer we compute the spectral correlation function by [1]

$$C(\Delta\lambda, D_i) = \frac{\langle I(\lambda, D_i) I(\lambda + \Delta\lambda, D_i) \rangle}{\langle I(\lambda, D_i) \rangle \langle I(\lambda + \Delta\lambda, D_i) \rangle} - 1, \quad (1)$$

where $I(\lambda, D_i)$ denotes the light intensity at wavelength λ and detector D_i ($i = 1, 2, \dots, 13$) and the average is taken over the wavelength. C is averaged over all detectors and normalized at

$\Delta\lambda = 0$. As a result, the half-width at half-maximum (HWHM) of the correlation function provides an estimate of the spectral resolution.

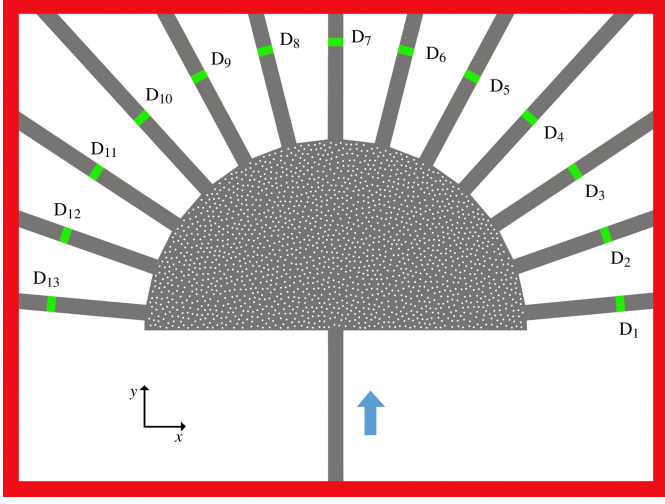


Fig. 1. (Color online) Schematic of the random spectrometer layout considered in this work. Radiation is launched into the center of the semicircular scattering area through an input waveguide and after multiple scattering reaches the 13 output waveguides where it is detected at the detectors D_1, \dots, D_{13} (green lines), or leaks into free space. Grey-shaded regions correspond to silicon nitride, white-shaded regions correspond to free space, and red-shaded regions represent perfectly matched layers that absorb any outgoing radiation. See text for further details.

Since the pore filling fraction is $f = 0.09$, multiple scattering can be treated via the independent scattering approximation [13, 14], where the multiple scattering process can be described by appropriate combinations of single-scattering quantities (we will touch upon the case of higher filling ratios below). The scattering efficiency for an infinite homogeneous cylindrical scatterer at normal incidence reads

$$Q_{sc}^{s,p} = \frac{2}{kR} \left[|a_0^{s,p}|^2 + 2 \sum_{n=1}^{\infty} |a_n^{s,p}|^2 \right], \quad (2)$$

where k is the wavenumber in the background material, R denotes the radius of the cylinder, a_n ($n = 0, 1, 2, \dots$) represent the Mie scattering coefficients. Finally, the superscripts s and p correspond, respectively, to s-wave (TM-polarization, electric field perpendicular to the xy -plane in Fig. 1) and p-wave (TE-polarization, electric field parallel to the xy -plane in Fig. 1). The associated differential scattering efficiency is

$$\frac{\partial Q_{sc}^{s,p}(\phi)}{\partial \phi} = \frac{2}{\pi k R} \left| a_0^{s,p} + 2 \sum_{n=1}^{\infty} a_n^{s,p} \cos(n\theta) \right|^2, \quad (3)$$

where $\theta = \pi - \phi$ is the scattering angle. The average cosine of the scattering angle defines [15, 16] the so-called asymmetry parameter g :

$$g^{s,p} = \langle \cos(\theta) \rangle = \frac{\int_0^\pi \frac{\partial Q_{sc}^{s,p}(\phi)}{\partial \phi} \cos(\theta) d\theta}{Q_{sc}^{s,p}} \quad (4)$$

$$= \frac{4}{k R Q_{sc}^{s,p}} \sum_{n=0}^{\infty} a_n^{s,p} (a_{n+1}^{s,p})^*.$$

For isotropic scattering, the asymmetry parameter vanishes and for predominantly forward (backward) scattering the asymmetry parameter takes on positive (negative) values. From multiple-scattering theory [17, 18] it follows that for lossless scatterers the transport mean free path is given by

$$l_t^{s,p} = \frac{\pi R}{2f Q_{sc}^{s,p} (1 - g^{s,p})} \quad (5)$$

within the independent scattering approximation [13, 14]. In the diffusive regime, the spectral resolution of random spectrometers scales as $l_t^{s,p}/L^2$ [19], so that reduced transport mean free paths $l_t^{s,p}$ are generally desirable. According to Eq. 5, short transport mean free paths can be expected when the (wavelength-dependent) scattering efficiency is high (strong scattering) and when the asymmetry parameter is significantly below 1 (near isotropic or even predominant backward scattering).

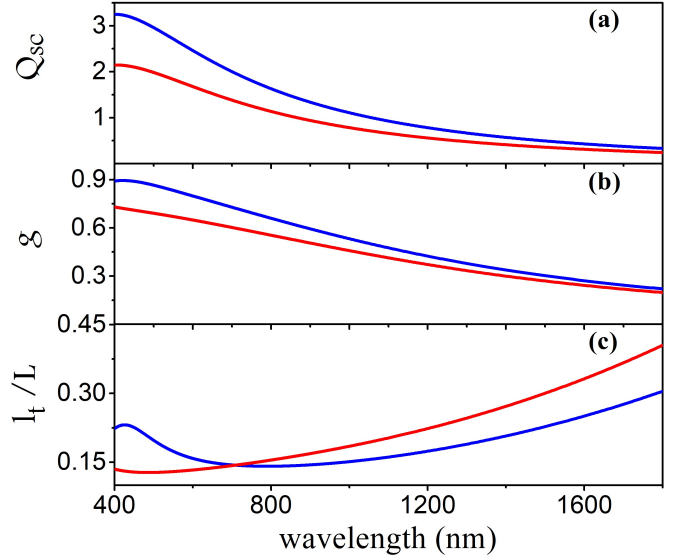


Fig. 2. (Color online) (a) Scattering efficiency Q_{sc} and (b) asymmetry parameter g of an air cylinder of radius 125 nm embedded in a silicon nitride matrix. The system is irradiated with s- and p-waves under normal incidence (blue and red lines, respectively). (c) Calculated transport mean free path l_t normalized to the radius L of the scattering area of a 2D disordered medium composed of air pores in a silicon nitride matrix where the pores occupy a fraction $f = 0.09$ of the available area.

For an air pore of 125 nm radius embedded in a silicon-nitride matrix, we display in Fig. 2 both, the scattering efficiency and the asymmetry parameter, for TE and TM polarization. We observe that when moving from telecom frequencies to visible frequencies, the scattering efficiencies increase monotonously while simultaneously the asymmetry parameter concurrently moves to even stronger forward scattering. Despite these opposing trends, the overall effect is that the transport mean free path reduces when moving from telecom to visible wavelengths (with a minimum around 700 nm for TE polarization) so that high spectral resolution of the random spectrometer is expected for the red end of the visible spectrum and NIR frequencies. Further reduction of the operation wavelength (~ 400 nm) would lead to an elongated transport mean free path for TE polarization due to a stronger increase in the forward scattering characteristics relative to the corresponding increase in the scattering efficiency.

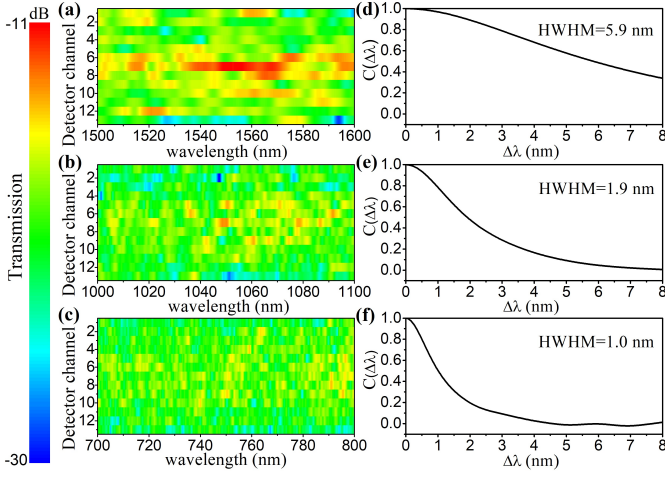


Fig. 3. (Color online) Panels (a), (b) and (c): Wavelength- and detector-resolved transmission matrix for the random spectrometer depicted in Fig. 1 for TE polarization for the visible, NIR and telecom wavelength region, respectively. Light is launched from the input port and is detected by the detectors D_1 to D_{13} . The ordinate labels correspond to the detector index. The color coding corresponds to the relative intensity transmitted into the different waveguides and expressed in decibels. Panels (d), (e) and (f): The normalized spectral correlation function corresponding to the wavelength regimes of panels (a), (b) and (c).

In Figs. 3 and 4, we display the wavelength- and detector-resolved transmission matrices for TE and TM polarization, respectively. As described above, these results have been obtained for the random spectrometer sketched in Fig. 1 by solving the Maxwell equations numerically using the DGTD upwind scheme approach [11]. Within this approach we use an adaptive tetrahedron mesh for the spatial discretization with a minimal element size of 4.7 nm and a polynomial order of 3. Meanwhile, the time-stepping is handled by a 14-stage fourth order low-storage-Runge scheme [12].

At telecom wavelengths (1500 nm-1600 nm), we find that the transport mean free path becomes comparable to the radius of the scattering area so that ballistic transport is dominant. As a result, the transmission matrix (Fig. 3(a) for TE polarization and Fig. 4(a) and (b) for TM polarization), is characterized by concentrations of the intensity in the central output ports (6-8).

Upon moving to NIR wavelengths (1000 nm-1100 nm) stronger multiple scattering occurs and we observe the onset of diffusion where the transmission matrix exhibits a more uniform distribution over the different output ports (cf. Fig. 3(b)), while at the same time the random spectrometer exhibits higher resolutions: Here, the HWHM is 1.9 nm for TE polarization and 2.1 nm for TM polarization, respectively, which is essentially less than half the values obtained at telecom wavelengths. Finally, we would like to note that the differences between TE and TM polarization in the angular distribution of light over the output ports can be explained by the angular characteristics of light scattering by a single scatterer (cf. Fig. 5). For TE polarization, scattering by p-waves is dominant and light scatters more into the forward direction so that it is primarily detected in the central output ports as long as the diffusive regime is not fully developed. For TM polarization, scattering by s-waves is dominant, which leads to more isotropic single-particle scattering and subsequently the

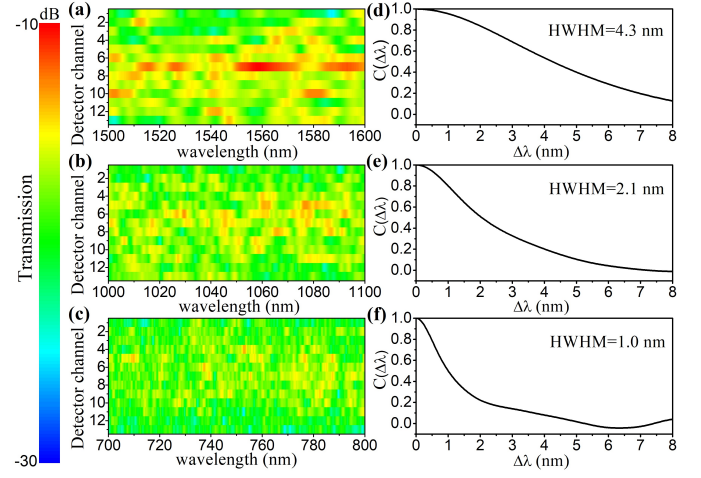


Fig. 4. (Color online) Panels (a), (b) and (c): Wavelength- and detector-resolved transmission matrix for the random spectrometer depicted in Fig. 1 for TM polarization for the visible, NIR and telecom wavelength region, respectively. Light is launched from the input port and is detected by the detectors D_1 to D_{13} . The ordinate labels correspond to the detector index. The color coding corresponds to the relative intensity transmitted into the different waveguides and expressed in decibels. Panels (d), (e) and (f): The normalized spectral correlation function corresponding to the wavelength regimes of panels (a), (b) and (c).

light is more evenly distributed over all output ports even if the diffusive regime is not fully developed (cf. Figs. 3(b) and 4(b)).

At the red end of the visible spectrum (700 nm-800 nm), we find that the transport mean free path is further reduced and the transmission matrix (Figs. 3(c) and 4(c)) is characterized by sharp peaks with a uniform spatial distribution, i.e., we find diffusive speckle patterns. For this wavelength range, the random spectrometer exhibits the highest resolution, 1.0 nm for both polarizations (see Figs. 3(f) and 4(f)).

Clearly, the above numerical results are in full agreement with the predictions of the combined Mie and multiple-scattering theory and demonstrate that the highest spectral resolution of the spectrometer is obtained when the diffusive regime is fully developed. However, acceptable resolution can already be obtained when the size of the scattering region just barely allows for the onset of diffusion. If ballistic transport is dominant, the spectral resolution will be lower. Thus, which transport regime to select, should, thus, be based on a compromise between desired resolution and available footprint of the device. At this point it should be noted that scattering from low-index inclusions in high-index matrices, quite generally, does not exhibit pronounced Mie resonances notably at low and moderate index contrasts. This suggests that our findings are of a rather general nature and, for instance, apply to other material systems such as ZnO, chalcogenides and LiNbO_3 and broad wavelength ranges.

In summary, through a combination of electrodynamic simulations, Mie theory and multiple-scattering theory, we have studied the response of planar random spectrometers in low-footprint integrated-optical layout for TE and TM polarization at telecom, NIR and visible wavelengths. We have shown that the attainable spectral resolution depends on the interplay of two single scattering properties, scattering efficiency and the asymmetry parameter. The highest resolution is obtained for systems

where the diffusive regime is fully developed. However, the transition regime between ballistic and diffusive transport might be sufficient for certain applications. These results are based on low filling fractions of the scatterers. For higher filling fractions, strong multiple-scattering corrections blur the connection to the single-scattering quantities. In this high- f regime, an effective medium theory capable of reliably determining transport mean free paths [20] can be employed instead of the independent scattering approximation. Our design study provides a basis for the realization of random spectrometers in the visible and NIR wavelength range.

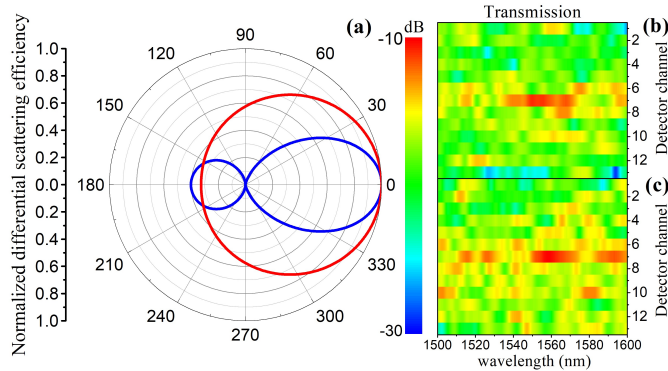


Fig. 5. (Color online) Panel (a): Angular scattering characteristics, Eq. (3), for an air pore of 125 nm radius embedded in a silicon nitride matrix, for TE (blue line) and TM (red line) polarizations and fixed wavelength $\lambda = 1500$ nm. Light scatters to larger angles for TM polarization due to predominance of s-wave scattering. Panels (b),(c): Wavelength- and detector-resolved transmission matrix for TE and TM polarizations, respectively.

FUNDING

We acknowledge support by the Deutsche Forschungsgemeinschaft (DFG) under project Bu 1107/10-1 within the framework of the DFG priority program SPP 1839 (*Tailored Disorder*).

REFERENCES

1. B. Redding, S. F. Liew, R. Sarma, and H. Cao, *Nature Photonics* **7**, 746 (2013).
2. A. Dhakal, F. Peyskens, S. Clemmen, A. Raza, P. Wuytens, H. Zhao, N. Le Thomas, and R. Baets, *Interface focus* **6**, 20160015 (2016).
3. A. Yodh and B. Chance, *Physics Today* **48**, 34 (1995).
4. S. Gayen and R. Alfano, *Optics and Photonics news* **7**, 16 (1996).
5. H. Zhao, B. Kuyken, S. Clemmen, F. Leo, A. Subramanian, A. Dhakal, P. Helin, S. Severi, E. Brainis, G. Roelkens, and R. Baets, *Optics letters* **40**, 2177 (2015).
6. D. J. Moss, R. Morandotti, A. L. Gaeta, and M. Lipson, *Nature Photonics* **7**, 597 (2013).
7. I. Goykhman, B. Desiatov, and U. Levy, *Applied Physics Letters* **97**, 081108 (2010).
8. A. Z. Subramanian, S. Selvaraja, P. Verheyen, A. Dhakal, K. Komorowska, and R. Baets, *IEEE Photonics Technology Letters* **24**, 1700 (2012).
9. S. Romero-García, F. Merget, F. Zhong, H. Finkelstein, and J. Witzens, *Optics express* **21**, 14036 (2013).
10. S. Romero-García, F. Merget, F. Zhong, H. Finkelstein, and J. Witzens, *Optics letters* **38**, 2521 (2013).
11. K. Busch, M. Koenig, and J. Niegemann, *Laser & Photonics Reviews* **5**, 773 (2011).

12. J. Niegemann, R. Diehl, and K. Busch, *Journal of Computational Physics* **231**, 364 (2012).
13. M. P. van Albada, B. A. van Tiggelen, A. Lagendijk, and A. Tip, *Physical review letters* **66**, 3132 (1991).
14. B. A. van Tiggelen, A. Lagendijk, M. P. van Albada, and A. Tip, *Physical review B* **45**, 12233 (1992).
15. H. C. Hulst and H. C. van de Hulst, *Light scattering by small particles* (Courier Corporation, 1957).
16. C. F. Bohren and D. R. Huffman, *Absorption and scattering of light by small particles* (John Wiley & Sons, 2008).
17. A. Ishimaru, *Wave propagation and scattering in random media*, vol. 2 (Academic press New York, 1978).
18. T. J. Arruda, A. S. Martinez, and F. A. Pinheiro, *Physical Review A* **94**, 033825 (2016).
19. D. Pine, D. Weitz, P. Chaikin, and E. Herbolzheimer, *Physical review letters* **60**, 1134 (1988).
20. A. Kirchner, K. Busch, and C. Soukoulis, *Physical Review B* **57**, 277 (1998).